# *Equilibrium behavior of symmetric ABA triblock copolymer melts*

# Equilibrium behavior of symmetric ABA triblock copolymer melts

M. W. Matsen and R. B. Thompson

Citation: The Journal of Chemical Physics **111**, 7139 (1999); doi: 10.1063/1.480006
View online: http://dx.doi.org/10.1063/1.480006
View Table of Contents: http://scitation.aip.org/content/aip/journal/jcp/111/15?ver=pdfcov
Published by the AIP Publishing



# Equilibrium behavior of symmetric ABA triblock copolymer melts

M. W. Matsen[a] and R. B. Thompson
*Polymer Science Center, University of Reading, Whiteknights, Reading RG6 6AF, United Kingdom*

(Received 16 June 1999; accepted 27 July 1999)

Melts of ABA triblock copolymer molecules with identical end blocks are examined using self-consistent field theory (SCFT). Phase diagrams are calculated and compared with those of homologous AB diblock copolymers formed by snipping the triblocks in half. This creates additional end segments which decreases the degree of segregation. Consequently, triblock melts remain ordered to higher temperatures than their diblock counterparts. We also find that middle-block domains are easier to stretch than end-block domains. As a result, domain spacings are slightly larger, the complex phase regions are shifted towards smaller A-segment compositions, and the perforated-lamellar phase becomes more metastable in triblock melts as compared to diblock melts. Although triblock and diblock melts exhibit very similar phase behavior, their mechanical properties can differ substantially due to triblock copolymers that bridge between otherwise disconnected A domains. We evaluate the bridging fraction for lamellar, cylindrical, and spherical morphologies to be about 40%–45%, 60%–65%, and 75%–80%, respectively. These fractions only depend weakly on the degree of segregation and the copolymer composition. © *1999 American Institute of Physics.* [S0021-9606(99)51139-2]

## I. INTRODUCTION

Block copolymers have received considerable attention due to the intriguing periodic ordered morphologies they exhibit. Much of this attention has been focused on the AB diblock copolymer because it has the simplest possible architecture. As a result, we have developed a very thorough understanding of its equilibrium behavior.[1,2] However, there are a wide variety of other flavors. AB-type block copolymers alone have been synthesized to form triblocks, linear multiblocks, combs, stars with diblock arms, hetero-arm stars, H-shaped copolymers, and various other architectures.[3] It is somewhat surprising that this rich selection of AB-type copolymers seems to exhibit the same common set of ordered morphologies displayed in Fig. 1. This includes the classical lamellar ($L$), cylindrical ($C$), and spherical ($S$) phases plus the complex gyroid ($G$) structure. Nevertheless, variations in the architecture do significantly shift the location of the phase boundaries.[4] They may also stabilize the perforated-lamellar (PL) phase, which in diblock copolymer melts is highly metastable in the region where $G$ is stable.[5]

To understand why changing the architecture of AB-type block copolymers has a limited effect on phase behavior, consider an ordered melt of symmetric ABA triblocks of polymerization $2N$ (see Fig. 2). If the melt is well segregated, then the polymer chains will stretch significantly in order to reduce the amount of interface. However, the middle of the B block, which is typically near the center of a B-rich domain, is relatively unstretched. Consequently, the free energy of the melt remains virtually unaffected if all the triblocks are snipped at this location producing a system of diblocks.[6] In fact, the phase behavior of ABA triblocks and their homologous AB diblocks of polymerization $N$ becomes identical in the strong-segregation limit.[7] Similar arguments can be applied to more complicated multiblock copolymers.

One distinct difference between the two architectures is that ABA triblocks have both ends of their B block constrained to an interface. Therefore, we can distinguish between looped and bridged configurations in morphologies where there are distinct interfaces (see Fig. 2). In a looped configuration, both ends of the B block reside on the same interface, but in a bridged configuration, the two ends lie on different interfaces. Although this issue has very little effect on the equilibrium phase behavior, the presence of bridges linking separate interfaces together strongly affects the mechanical properties of the material.[8,9] In fact, bridges are a crucial aspect of thermoplastic elastomers, which are one of the most successful applications of block copolymers.

There has already been a considerable amount of research directed towards ABA triblock copolymer melts. Early on, Helfand and Wasserman[6] predicted that the phase behavior of homologous triblock and diblock melts would be nearly identical at strong segregations. Indeed, experiments commonly observe the same three classical phases, $L$, $C$, and $S$, as found in diblock melts. Furthermore, recent experiments[10] have identified gyroid phases on both sides of the triblock lamellar region, suggesting that the complex phase behavior is also the same. Matsushita *et al.*[11] have confirmed that the lamellar domain spacings of homologous triblock and diblock melts are similar, although accurate experiments of Mai *et al.*[12] have recently found the spacings to be slightly larger in the triblock system. Mayes and Olvera de la Cruz have calculated the mean-field phase boundaries in the weak-segregation limit[13] and have subsequently computed fluctuation corrections.[14] Although their triblock phase diagram is topologically the same as that for diblocks, it does predict a significant shift in the order–disorder transition (ODT). This has since been confirmed by numerous experi-

[a]Author to whom correspondence should be addressed.

 

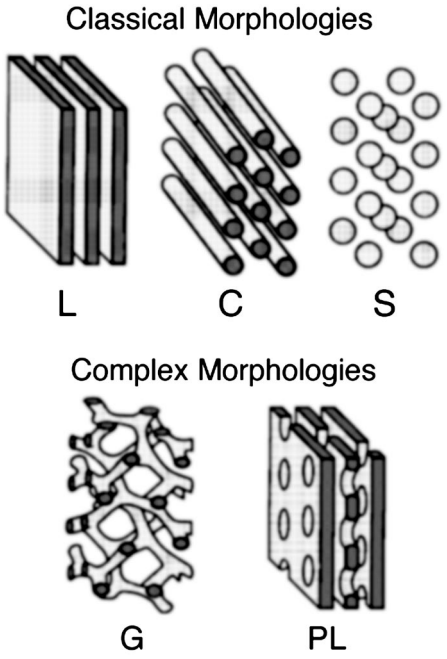


FIG. 1. Illustrations of AB-type block copolymer microstructures showing the domains occupied by the minority-component blocks. The remaining space is filled by the majority-component blocks.

mental groups.[8,12] Despite such similar phase behavior, various experiments[8,9] have documented large mechanical differences indicating that triblock copolymers commonly adopt bridged configurations. Indeed, theoretical calculations[7,15] have predicted the bridging fraction in the lamellar morphology to be about 40%. Watanabe[16] has since confirmed this experimentally.

Recent developments[17,18] in self-consistent field theory (SCFT) have now made it possible to apply exact mean-field theory to block copolymer melts over the complete spectrum of segregations.[19] Such calculations have already been used to provide detailed explanations for AB diblock copolymer phase behavior.[1,2] Here, we now apply this state-of-the-art theory to symmetric ABA triblock copolymer melts. The SCFT is used to examine phase diagrams, segment distributions, interfacial widths, domain spacings, and bridging fractions. Our study also includes detailed comparisons between ABA triblock melts and homologous AB diblock melts in an effort to better understand how architecture affects phase behavior.

## II. THEORY

This section briefly describes the self-consistent field theory (SCFT) (Refs. 17–20) for a monodisperse melt of $n$ symmetric ABA triblock copolymers. Each triblock molecule is composed of $2N$ segments of which $f_A N$ form each A block and the remaining $2(1-f_A)N$ form the middle B block. The A and B segments are assumed to be incompressible and are defined based on a common segment volume $\rho_0^{-1}$, so that the total volume of the melt remains fixed at $\mathcal{V}=2nN/\rho_0$. The A and B segments are also assumed to be completely flexible with statistical lengths $a_A$ and $a_B$, respectively;[21] i.e., the unperturbed rms end-to-end length of

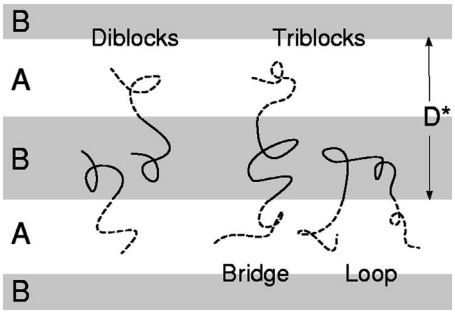


FIG. 2. Typical configurations of AB diblock and ABA triblock copolymers in a lamellar morphology. Triblock molecules are shown in both bridge- and loop-type configurations.

a triblock molecule is $a(2N)^{1/2}$, where $a\equiv(f_A a_A^2+(1-f_A)a_B^2)^{1/2}$. The interaction between A and B segments is controlled by the usual Flory–Huggins $\chi$ parameter. We parameterize the contour of each copolymer by $s$, which increases from 0 to 2 over the length of the molecule. This allows us to define

$$\nu(s)=\begin{cases} A, & \text{if } 0<s<f_A, \\ B, & \text{if } f_A<s<2-f_A, \\ A, & \text{if } 2-f_A<s<2, \end{cases} \tag{1}$$

to specify the segment type along the chain. Furthermore, the parameterization allows us to define the space curve $\mathbf{r}_\alpha(s)$ in order to specify the configuration of the $\alpha$th copolymer.

In SCFT, the molecular interactions are represented by two static fields, $w_A(\mathbf{r})$ and $w_B(\mathbf{r})$, which act on the A and B segments, respectively. This mean-field approximation allows us to perform the statistical mechanics of a triblock copolymer exactly. The first step in this process is to evaluate

$$q(\mathbf{r},s)=\int \mathcal{D}\mathbf{r}_\alpha \delta(\mathbf{r}-\mathbf{r}_\alpha(s)) \times\exp\left\{-\int_0^s dt\left[\frac{3}{2Na_{\nu(t)}^2}\left|\frac{d}{dt}\mathbf{r}_\alpha(t)\right|^2 + w_{\nu(t)}(\mathbf{r}_\alpha(t))\right]\right\}, \tag{2}$$

which is the partition function for the $(0,s)$ portion of the chain with the $s$th segment fixed at position $\mathbf{r}$. The two terms in the exponential represent the entropy loss for stretching the chain and the energy resulting from the fields, respectively. This function conveniently satisfies the modified diffusion equation,

$$\frac{\partial}{\partial s}q(\mathbf{r},s)=\left[\tfrac{1}{6}Na_{\nu(s)}^2\nabla^2-w_{\nu(s)}(\mathbf{r})\right]q(\mathbf{r},s), \tag{3}$$

with the initial condition $q(\mathbf{r},0)=1$.[17]

The product $q(\mathbf{r},s)q(\mathbf{r},2-s)$ provides the partition function for a complete triblock molecule with its $s$th segment constrained to position $\mathbf{r}$. Summing this over all possible positions provides the partition function for an unconstrained triblock,

$$\mathcal{Q}=\int d\mathbf{r}q(\mathbf{r},s)q(\mathbf{r},2-s). \tag{4}$$

This integral is independent of $s$ as it must be. Furthermore, $q(\mathbf{r},s)q(\mathbf{r},2-s)$ is proportional to the distribution function $\rho(\mathbf{r},s)$ for the $s$th segment. If we choose to normalize the distribution so that its average is one, then

$$\rho(\mathbf{r},s)=\frac{\mathcal{V}}{\mathcal{Q}}q(\mathbf{r},s)q(\mathbf{r},2-s). \tag{5}$$

Given that, it follows that the total A and B segment distributions are

$$\phi_A(\mathbf{r})=\frac{\mathcal{V}}{\mathcal{Q}}\int_0^{f_A}dsq(\mathbf{r},s)q(\mathbf{r},2-s), \tag{6}$$

$$\phi_B(\mathbf{r})=\frac{\mathcal{V}}{\mathcal{Q}}\int_{f_A}^{1}dsq(\mathbf{r},s)q(\mathbf{r},2-s), \tag{7}$$

respectively, where we have used the fact the triblock molecule is symmetric about its middle (i.e., $s=1$).

The fields are produced by and thus are related to the segment distributions by self-consistent field equations,[18]

$$w_A(\mathbf{r})=\chi N\phi_B(\mathbf{r})+\xi(\mathbf{r}), \tag{8}$$

$$w_B(\mathbf{r})=\chi N\phi_A(\mathbf{r})+\xi(\mathbf{r}). \tag{9}$$

In both expressions, the first term represents the segment interactions, and the last term is a Lagrange multipler used to enforce the incompressibility constraint,

$$\phi_A(\mathbf{r})+\phi_B(\mathbf{r})=1. \tag{10}$$

These equations are satisfied by adjusting the fields using a quasi-Newton–Raphson method. There are multiple solutions each representing a different phase. The stable phase is the one with the lowest free energy $F$ given by

$$\frac{F}{2nk_BT}=-\frac{1}{2}\ln\frac{\mathcal{Q}}{\mathcal{V}}-\frac{\chi N}{\mathcal{V}}\int d\mathbf{r}\phi_A(\mathbf{r})\phi_B(\mathbf{r}). \tag{11}$$

For the uniform disordered phase, this expression reduces to $F/2nk_BT=\chi Nf_A(1-f_A)$. If the phase is ordered, $F$ has to be minimized with respect to the domain spacing. All the ordered phases considered in this study are periodic, and therefore we solve their equations using the Fourier method in Ref. 18 with up to 400 basis functions.

It is a straightforward calculation to determine the equilibrium fraction of triblocks existing in bridged and looped configurations (see Fig. 2). The first step is to evaluate the partition function,

$$\overline{q}(\mathbf{r},f_A)=\begin{cases}q(\mathbf{r},f_A), & \text{if } \mathbf{r}\in 1\text{st cell},\\ 0, & \text{otherwise},\end{cases} \tag{12}$$

for an A block with its $s=f_A$ junction constrained to the first unit cell. By propagating this with the modified diffusion Eq. (3), we obtain the partition function $\overline{q}(\mathbf{r},s)$ for the $(0,s)$ portion of a chain with the first junction constrained to the first unit cell and the $s$th segment ($s\geqslant f_A$) fixed at position $\mathbf{r}$. [Because $\overline{q}(\mathbf{r},s)$ is not periodic, it is calculated in real space using the Crank–Nicolson algorithm.] We can then evaluate the distribution $\overline{\rho}(\mathbf{r},s)$ of the $s$th segment ($s\geqslant f_A$) from all the triblocks with their first junction in the first unit cell using

$$\overline{\rho}(\mathbf{r},s)=\frac{\mathcal{V}}{\mathcal{Q}}\overline{q}(\mathbf{r},s)q(\mathbf{r},2-s). \tag{13}$$

These triblocks form loops provided their second junction is also in the first unit cell, and thus the fraction of looped configurations is

$$\nu_L=\frac{1}{\mathcal{V}_{\text{cell}}}\int_{1\text{st cell}}d\mathbf{r}\overline{\rho}(\mathbf{r},2-f_A), \tag{14}$$

where $\mathcal{V}_{\text{cell}}$ is the volume of a unit cell. Naturally, the remaining triblocks must form bridges, and therefore the bridging fraction is $\nu_B=1-\nu_L$.

## III. RESULTS

The phase diagrams in Fig. 3 for symmetric ABA triblock copolymer melts are evaluated by comparing the free energies of the disordered phase and each ordered phase shown in Fig. 1. Diagrams are presented for three different statistical segment length ratios. In each case, the topology of the diagram is equivalent to that of the standard AB diblock system.[1,2] The sequence of ordered phases from the middle ($f_A\approx 0.5$) outwards is lamellae ($L$), gyroid ($G$), hexagonal cylinders ($C$), body-centered-cubic spheres ($S$), and close-packed spheres ($S_{\text{cp}}$). All three classical phases, $L$, $C$, and $S$, extend upwards from mean-field critical points denoted by solid dots, but the $G$ and $S_{\text{cp}}$ regions do not begin until the melt becomes well segregated. Presumably, the $G$ regions eventually pinch off at high segregations as a result of packing frustration,[1,2] but we could not confirm this due to numerical limitations that prevented us from calculating the free energy of $G$ accurately at strong segregations. This is the reason that some of the phase boundaries in Fig. 3 had to be extrapolated with dashed lines. The $S_{\text{cp}}$ phase, however, is expected to extend to the strong-segregation limit in narrow regions along the order–disorder transition (ODT). These regions occur when the thermal energy is sufficient to pull a significant fraction of minority blocks from their spherical domains. This swells the matrix, which relieves packing frustration and allows the spheres to order into a close-packed lattice as favored by the effective interactions between them.[22] The mean-field phase diagrams in Fig. 3 are modified somewhat along the ODT by fluctuation effects, which will be discussed in the next section.

The perforated-lamellar (PL) phase competes closely with the $G$ phase for stability, because it has a similar degree of interfacial curvature.[1,2] However, the PL phase possesses slightly more packing frustration, and consequently it remains unstable relative to the $G$ phase.[1,2] Nevertheless, its high degree of metastability is sufficient that it can persist for extremely long periods of time before converting to the $G$ morphology.[5] Figure 4 examines the free energy difference $\Delta F_{\text{PL}}$ between the PL and $G$ phases along the $G/L$ phase boundary. PL is most metastable along this side of the $G$ regions, because its interfacial curvature is slightly less than that of $G$. The plots demonstrate that the PL phase is far

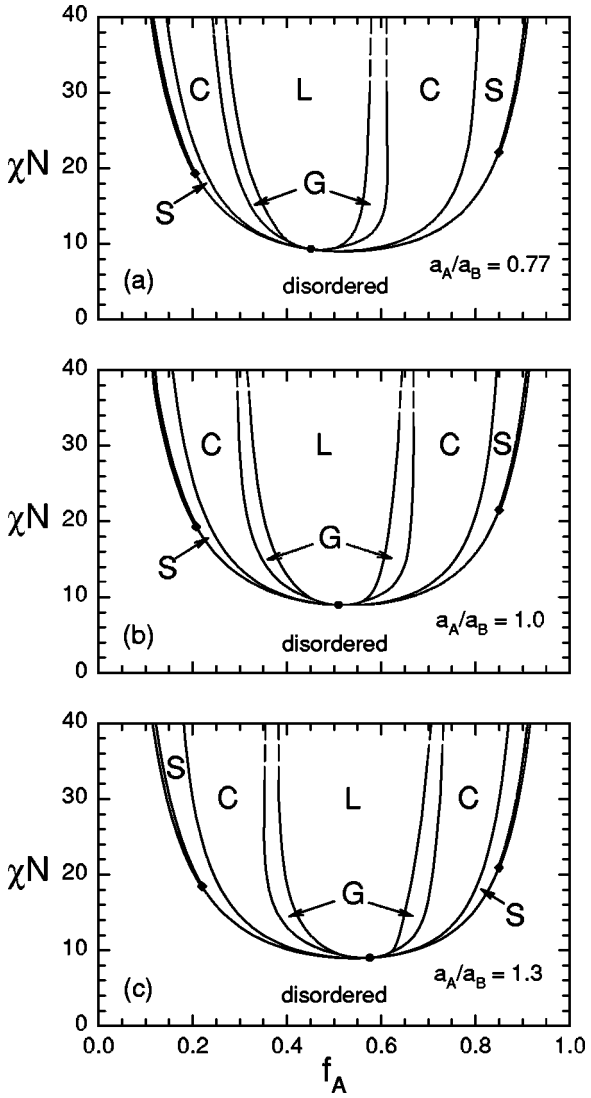


FIG. 3. Mean-field phase diagrams for symmetric ABA triblock copolymers of polymerization $2N$ for a selection of statistical segment length ratios. The ordered phases are labeled as $L$ (lamellar), $G$ (gyroid), $C$ (cylindrical), and $S$ (spherical). Above the solid diamonds along the order-disorder transition (ODT) are narrow regions where the $S_{cp}$ (close-packed spherical) phase is stable. The solid dots denote mean-field critical points, and the dashed curves are extrapolated phase boundaries.

more metastable on the small-$f_A$ side of the phase diagram, where the outer A blocks form the perforated lamellae. Also, an appropriate conformational asymmetry increases its metastability just as it does in the diblock system.[21] It is quite possible that a higher level of asymmetry could, in fact, stabilize the PL phase.

The interfacial width $w$ between A and B domains is a good indicator of the degree of segregation. Figure 5 compares the interfacial widths in an $f_A=0.5$ ABA triblock melt and its AB diblock counterpart as a function of $\chi N$. (We define the width as $w\equiv(d\phi_A/dz)^{-1}$ evaluated at the interface.)[19] The width is generally narrower in the triblock system indicating a higher level of order. To understand how snipping triblocks in half reduces the segregation, we examine segment profiles $\rho(z,s)$ in an $f_A=0.5$ lamellar phase, where $z$ is the coordinate orthogonal to the lamellae. The solid curves in Fig. 6 show the profiles of the first junction

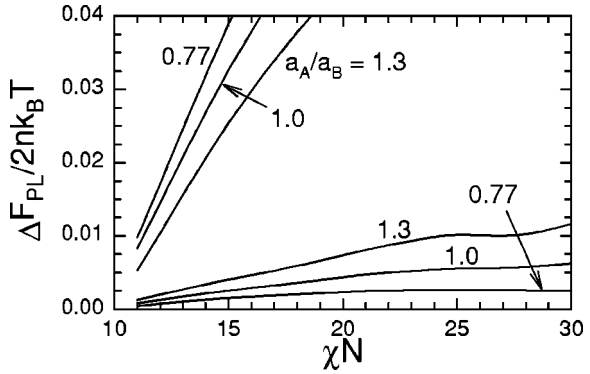


FIG. 4. Excess free energy $\Delta F_{PL}$ of the perforated-lamellar (PL) phase along the $L/G$ phase boundary for the three statistical segment length ratios considered in Fig. 3. The upper and lower sets of curves correspond to the large-$f_A$ and small-$f_A$ sides, respectively, of the phase diagrams in Fig. 3.

$(s=f_A)$ and of the middle segment $(s=1)$. The dashed curves then show how these two distributions change for a triblock snipped at its midpoint (i.e., diblock segment distributions are calculated in the fields for the triblock melt). While the junction distribution is nearly unaffected, the middle segment distribution of the triblock broadens significantly when it becomes the end segment of a diblock. Although this effect will diminish in the strong-segregation limit, comparing the $\chi N=15$ and 30 results indicates that the effect remains significant to very high values of $\chi N$ even though it stops influencing the interfacial width by $\chi N \approx 30$.

Figure 7 compares the domain spacings in triblock melts (solid curves) to those in diblock melts (dashed curves). The top plot shows the domain spacing $D^*$ of an $f_A=0.5$ lamellar phase as a function of segregation $\chi N$, and the lower plot examines $D^*$ as a function of composition $f_A$. To compare spacings in different morphologies, we define $D^*\equiv 2\pi/q^*$, where $q^*$ is the principal wave vector. There are discontinuous jumps in $D^*$ at each phase transition consistent with experimental observations in both triblock and diblock melts.[9] In general, the period of a triblock morphology is about 5% greater than that in the corresponding diblock melt. Unlike the small difference observed in the interfacial widths $w$, this difference persists to very high degrees of segrega-

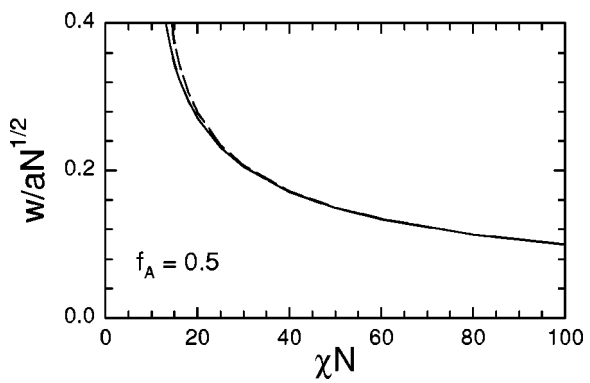


FIG. 5. Interfacial width $w$ plotted as a function of segregation $\chi N$ in an $f_A=0.5$ lamellar phase. The solid curve corresponds to triblocks of polymerization $2N$, and the dashed curve is for diblocks of polymerization $N$.

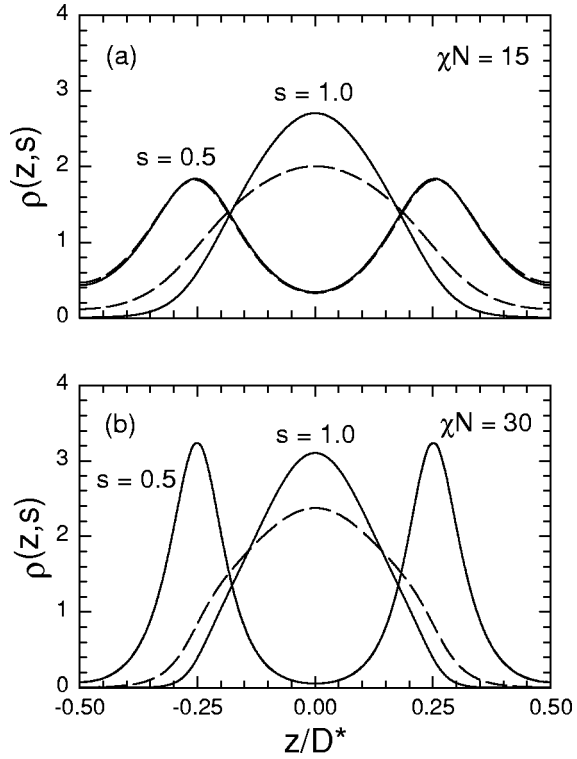


FIG. 6. Segment distributions $\rho(z,s)$ plotted over one period of an $f_A=0.5$ lamellar phase at (a) $\chi N=15$ and (b) $\chi N=30$. The solid and dashed curves are calculated for ABA triblock and AB diblock copolymers, respectively. The $s=0.5$ junction distributions are virtually identical, but the $s=1.0$ distributions, comparing the middle of a triblock and a B-end of a diblock, are considerably different.

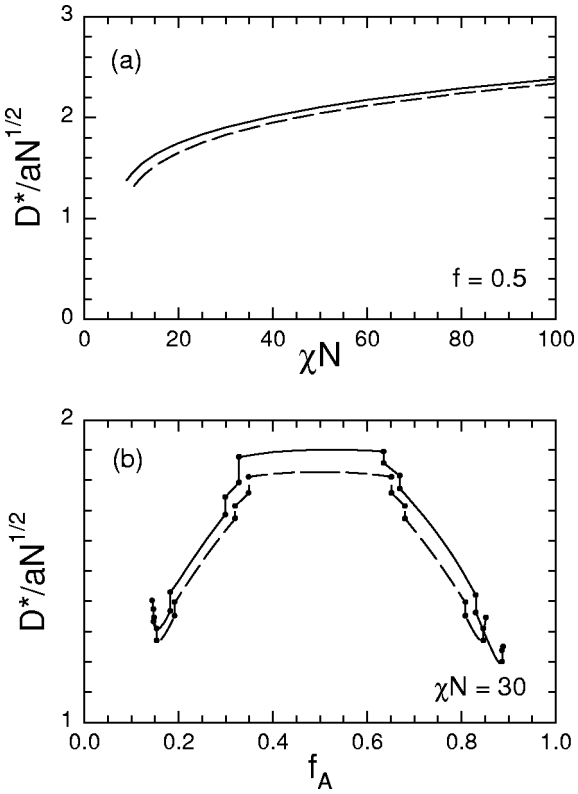


FIG. 7. Principal domain spacings $D^*$ as a function of (a) segregation $\chi N$ at fixed $f_A=0.5$ and of (b) composition $f_A$ at fixed $\chi N=30$. The solid curves correspond to triblocks of polymerization $2N$, and the dashed curves are for diblocks of polymerization $N$. In (b), the solid dots denote phase transitions, where $D^*$ changes discontinuously. For the $L$ phase the layer spacing equals $D^*$, for $G$ the size of the cubic unit cell is $6^{1/2}D^*$, for $C$ the spacing between cylinders is $(4/3)^{1/2}D^*$, and for $S$ and $S_{cp}$ the nearest-neighbor spacing of spheres is $(3/2)^{1/2}D^*$.

tion. Notice that in both systems, the spacing in the spherical phases increases sharply as the ODT is approached; this is due to minority blocks pulling free of their domains and swelling the matrix as discussed above.

A previous SCFT calculation[7] has calculated the bridging fraction $\nu_B$ in the $L$ morphology. Here, we extend that calculation to evaluate the fraction of B blocks that bridge between A-rich cylinders and spheres in the $C$, $S$, and $S_{cp}$ phases (*i.e.*, the small-$f_A$ side of the phase diagrams in Fig. 3). The procedure is illustrated in Fig. 8 for the $L$ and $C$ morphologies. The first step is to determine the $s=f_A$ junction distribution $\overline{\rho}(\mathbf{r},f_A)$ from a single minority A domain as displayed in Figs. 8(a) and 8(c). This distribution is then propagated as described in Sec. II to obtain the distribution $\overline{\rho}(\mathbf{r},2-f_A)$ of the connected $s=2-f_A$ junctions as shown in Figs. 8(b) and 8(d). The looping fraction $\nu_L$ is determined by integrating the volume under $\overline{\rho}(\mathbf{r},2-f_A)$ remaining in the initial unit cell. The bridging fraction is then given by $\nu_B=1-\nu_L$. Figure 9 shows the bridging fraction $\nu_B$ calculated as a function of $f_A$ for three values of $\chi N$. As determined earlier for the $L$ phase,[7,15] $\nu_B$ only depends weakly on the segregation and composition of the melt. However, $\nu_B$ changes significantly with morphology, except at the $S$ to $S_{cp}$ transition where the change is not noticeable on the scale of Fig. 9.

## IV. DISCUSSION

The same general principles that govern the behavior of AB diblock copolymer melts apply equally to ABA triblock copolymer melts, and consequently their phase diagrams are very similar. First of all, the same competition between A/B interfacial tension and chain stretching selects the domain size. Just as in diblock melts, a competition between the stretching energies of the A and B blocks produces a preferred curvature in the A/B interface. This preferred curvature increases in magnitude as $f_A$ deviates from $\sim 0.5$, which causes the system to select morphologies with more and more interfacial curvature. The ratio of the statistical segment lengths also affects the preferred curvature.[21] Decreasing $a_A/a_B$ makes B blocks easier to stretch relative to A blocks, which favors B on the inside of curvature and therefore causes a shift in the phase boundaries towards lower $f_A$ (see Fig. 3). Between the classical lamellar ($L$) and cylindrical ($C$) phases, numerous complex phases possess appropriate interfacial curvature, and thus they compete for stability.[1,2] As in the diblock system, the triblock melt selects the gyroid phase,[10] because it is best able to simultaneously produce interfaces of uniform curvature and domains of uniform thickness.[1,2] These tendencies are a result of interfacial tension and chain stretching, respectively.

Although the phase behavior of symmetric ABA tri-

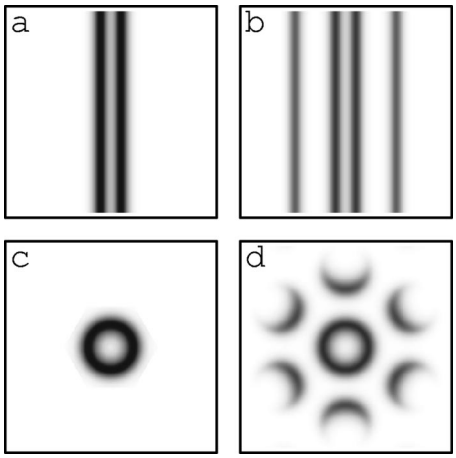


FIG. 8. Density plots of the segment distributions $\overline{\rho}(\mathbf{r},s)$ from triblock copolymers with their $s=f_A$ junctions confined to a particular minority A domain. The top two plots are for a lamellar morphology ($\chi N=30$ and $f_A=0.328$), and the bottom two are for a cylinder morphology ($\chi N=30$ and $f_A=0.299$). The left two plots are distributions of the $s=f_A$ junctions, and the right two are distributions of their associated $s=2-f_A$ junctions. The bridging fraction $\nu_B$ is obtained by appropriately integrating the distributions in (b) and (d).

blocks and AB diblocks is very similar, SCFT does predict several significant differences. This is evident in Figs. 5, 6, and 7 for the interfacial width, segment distributions, and domain spacings, respectively. Figure 10 also demonstrates significant shifts in the phase boundaries between homologous triblock and diblock phase diagrams. All these differences are reasonably straightforward to explain.

Snipping triblocks in half turns middle segments into end segments. This is particularly important at weak segregations, where B blocks can significantly penetrate A-rich domains. In this regime, the B end of a diblock can enter an A domain more easily than the middle B segment of a triblock, because the end segment only has to drag half as much B chain into the domain. Consequently, triblock melts remain ordered down to lower $\chi N$ than their homologous

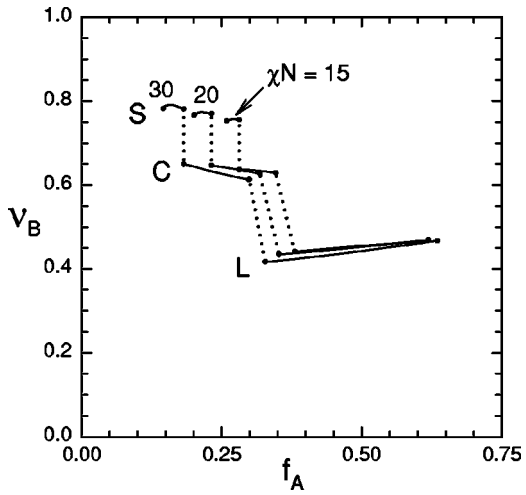


FIG. 9. Bridging fraction $\nu_B$ as a function of copolymer composition $f_A$ at $\chi N=15$, 20, and 30. The upper, middle, and lower curves correspond to the *S*, *C*, and *L* phases, respectively. The solid dots denote phase transitions, and the dotted lines are simply there to connect curves of the same $\chi N$.

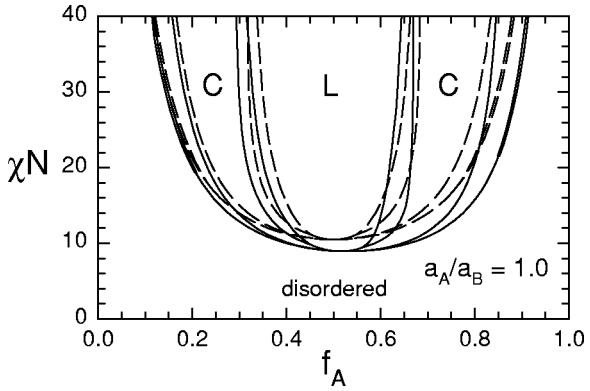


FIG. 10. Diblock copolymer phase diagram (dashed curves) overlaid on the triblock copolymer phase diagram (solid curves) from Fig. 3(b).

diblock counterparts. This effect is far more pronounced on the large-$f_A$ side of the phase diagram, because this is where the morphologies disorder as a result of B blocks pulling free of their domains. On the other side, the ODT occurs primarily as a result of A blocks coming free of their domains, and since both architectures have equivalent A blocks, their ODT's are nearly the same.

The slightly higher segregation in triblock melts causes their interfacial width to be narrower relative to diblock melts, however, the difference becomes negligible beyond $\chi N\approx 30$. Contrary to this prediction, an experiment by Anastasiadis *et al.*[23] found the interface in a highly segregated triblock melt to be 38% narrower. Unfortunately, their triblocks and diblocks were of equal size, which is not the most useful comparison. When compared at the same degree of polymerization $N$, SCFT predicts triblocks to have a wider interface, but with a difference that depends significantly on $\chi N$. For the estimated $\chi N=110$ in Ref. 23, SCFT predicts the triblock interface to be 5.9% wider. The situation improves slightly when the SCFT prediction is corrected for interfacial fluctuations.[24,25] Since the diblock melt has a larger period (when the copolymers are compared on an equal size basis), its interface will be broadened more by fluctuations. Nevertheless, the fluctuation correction does not even come close to accounting for the 38% difference. Since past comparisons between experiments and fluctuation-corrected SCFT predictions have been very impressive,[24,26] we are lead to question the accuracy of Ref. 23. Their experiment required inverting neutron reflectivity data, which relies on their assumptions regarding the segment profile. They apparently assume that all the interfaces in their thin film have the same width, when in fact the widths should decrease near the film surface.[27] An assumption such as this, coupled with the fact that reflectivity experiments are not particularly sensitive to the details of the interfacial profile, could be sufficient to explain this apparent disagreement between theory and experiment. We note that another analogous experiment[28] on a nearly identical triblock copolymer reported a far thinner interfacial width. Although this does not improve the situation, it does stress that the interpretation of neutron reflectivity data can be unreliable. Hopefully, future experiments will reexamine this issue, next time comparing homologous triblock and diblock pairs.

Away from the ODT, the ordered triblock melt becomes well segregated and behaves very similarly to its diblock counterpart. Both have virtually equivalent A domains and nearly identical A/B interfacial profiles. The only significant difference lies in the elastic properties of their B-rich domains. Evidently the B domains in a triblock melt are slightly softer (i.e., easier to stretch) than those of the diblock melt formed by snipping all the B blocks in half. Although the explanation for this is not obvious, the conclusion is well supported by our results.

One clear consequence of the softer B-rich domains is that the triblock morphologies have slightly larger domain spacings (on the order of 5%) than the analogous diblock morphologies (see Fig. 7). Early experiments[11] established that the lamellar spacing in $f_A=0.5$ triblock melts is similar to that of homologous diblock melts, but they did not detect the small difference predicted in Fig. 7(a). However, accurate measurements by Mai *et al.*[12] have recently observed a difference in the lamellar spacing, which is in excellent agreement with our SCFT prediction.

When the B domain becomes softer, the interface will tend to curve towards it. Although this requires the B blocks to stretch, that is more than compensated for by the fact the A blocks can relax. This change in preferred curvature causes the gyroid regions of the triblock system to shift towards lower $f_A$ relative to those of the diblock system (see Fig. 10). Note that this is the same shift that occurs in Fig. 3 when $a_A/a_B$ decreases, and furthermore the explanation is precisely the same.

Previous calculations[1,2] have demonstrated that the PL phase is slightly less stable than the *G* phase because of packing frustration in its majority domain. Packing frustration occurs when certain regions in the domain require excessive chain stretching. Naturally, the packing frustration will be reduced when the majority domain becomes softer. In agreement with this hypothesis, the PL phase is far more metastable on the small-$f_A$ side of the phase diagram where B forms the majority domain. Also note that this metastability increases when the majority domain is made even softer by changing the ratio $a_A/a_B$.

In triblock morphologies with isolated A-rich domains, the bridging fraction $\nu_B$ is of particular interest, because of its strong influence on the mechanical properties.[8,9] The bridging fraction in the lamellar phase (*L*) has been calculated using the Scheutjens–Fleer lattice SCFT,[15] the Semenov strong-segregation theory,[7] and the Helfand SCFT.[7] All three methods predict bridging fractions of ~40%, which is consistent with experimental measurements.[16] Li and Ruckenstein[29] have since calculated equilibrium bridging fractions in the *L*, *C*, and *S* phases using an alternative lattice theory. Their approach also considers chain stiffness, but this is of minor importance for high-molecular-weight polymers. However, it is troubling that the predictions in Ref. 29 are far lower than those calculated here and elsewhere; for example, they only predict a ~18% bridging fraction for the *L* phase as compared to the well established value of ~40%. Considering that the SCFT used here is an exact mean-field theory that, for example, determines the shape and size of the domains by minimizing the free energy and properly accounts for the two- and three-dimensional geometries of the *C* and *S* phases, respectively, there is virtually no doubt that the present calculation is more reliable.

The only inherent deficiency of SCFT is that it neglects several fluctuation effects, but in polymeric systems these are generally of minor importance, and furthermore they are well understood. The small interfacial fluctuations in well segregated melts, discussed above, can be treated as in Refs. 25 and 26 or by the more sophisticated method of Shi *et al.*[30] Fluctuations may also destroy the long-range order in the $S_{cp}$ phase, because the spheres are so weakly bound.[1] This would be consistent with recent experiments[31] that observe closely-packed spheres in the disordered phase just before it orders into the bcc spherical phase. The most notable effect of fluctuations occurs at weak segregations. Leibler[32] originally noted that because the disordered-state structure function diverges on a sphere, Brazovskii-type[33] fluctuations would destroy the weakly-ordered morphologies pushing the ODT to higher $\chi N$. Fredrickson and Helfand[34] later accounted for these fluctuations using the mean-field Landau free energy functional derived by Leibler. Since then, Mayes and Olvera de la Cruz[14] have repeated the calculation for triblocks. Although these calculations have greatly improved our understanding of Brazovskii fluctuations, they may be quantitatively unreliable given that they use the mean-field Landau free energy, which is inaccurate at weak segregations. Inconsistencies between Flory–Huggins $\chi$ parameters as measured from the ODT's of polymer blends and diblock copolymer melts have recently been attributed to this.[35] This suggests the need for a more rigorous fluctuation correction along the lines proposed by Stepanow.[36] Nevertheless, we have to consider other possible explanations for the inconsistent $\chi$ parameters, since issues such as chain stiffness[37] and small nematic interactions[38] can have a significant effect on the ODT's.

## V. CONCLUSIONS

We have investigated effects of block copolymer architecture by comparing the equilibrium phase behavior of symmetric ABA triblock copolymers of polymerization $2N$ to that of AB diblock copolymers of polymerization $N$. The presence of B ends in diblock melts reduces the segregation, and thus the triblock melts remain ordered down to lower values of $\chi N$. This is particularly true at large $f_A$, where the melt disorders due to the small energy required to dislodge B blocks from their domains. For well segregated melts, the A-rich domains and the A/B interfaces are virtually identical in the triblock and diblock systems. The only significant difference is that the B-rich domains are slightly softer in triblock melts. As a consequence, triblock morphologies have larger domain spacings, their complex phase regions are shifted to smaller $f_A$, and their PL phase is more metastable when B forms the majority domain.

Although the equilibrium behavior of homologous triblock and diblock melts is very similar, the mechanical properties can differ substantially in morphologies where ABA triblocks can bridge between distinct A-rich domains. Theory[7,15] has previously established that about 40%–45% of triblocks form bridges in the *L* phase. Here, we calculate a

bridging fraction of about 60%–65% in the $C$ phase and about 75%–80% in the $S$ and $S_{cp}$ phases. For a given morphology, the bridging fraction only depends weakly on segregation and copolymer composition.

Experiments have already supported a number of the SCFT predictions. For example, the bridging fraction in the lamellar phase has been measured to be ~40%. Furthermore, experiments[10] have located stable gyroid ($G$) phases on both sides of the triblock lamellar phase. Various comparisons[8,12] between homologous triblocks and diblocks have confirmed the predicted shift in the ODT (see Fig. 10). Furthermore, Mai *et al.*[12] have observed the slightly elevated lamellar spacing predicted for triblocks in Fig. 7. Mai and co-workers are also conducting experiments that will determine whether the complex phase regions in triblock melts are shifted relative to those of diblock melts as predicted in Fig. 10. Still, further experiments are required to establish complete confidence in our SCFT predictions. In particular, the interfacial widths should be reexamined given the apparent disagreement with experiment.[23] Detailed studies of this nature will improve our general understanding of how architecture affects phase behavior, and this will give us the ability to anticipate the behavior of more complicated block copolymers.

## ACKNOWLEDGMENTS

This work was supported by a NUF-NAL grant from the Nuffield Foundation and by the Engineering and Physical Sciences Research Council (GR/M18034).

[1] M. W. Matsen and F. S. Bates, J. Chem. Phys. **106**, 2436 (1997).
[2] M. W. Matsen and F. S. Bates, Macromolecules **29**, 7641 (1996).
[3] I. W. Hamley, *The Physics of Block Copolymers* (Oxford University Press, Oxford, 1998).
[4] S. T. Milner, Macromolecules **27**, 2333 (1994); M. W. Matsen and M. Schick, *ibid.* **27**, 6761 (1994).
[5] D. A. Hajduk, H. Takenouchi, M. A. Hillmyer, F. S. Bates, M. E. Vigild, and K. Almdal, Macromolecules **30**, 3788 (1997); M. E. Vigild, K. Almdal, K. Mortensen, I. W. Hamley, J. P. A. Fairclough, and A. J. Ryan, *ibid.* **31**, 5702 (1998).
[6] E. Helfand and Z. R. Wasserman, Macromolecules **9**, 879 (1976).
[7] M. W. Matsen, J. Chem. Phys. **102**, 3884 (1995).
[8] M. D. Gehlsen, K. Almdal, and F. S. Bates, Macromolecules **25**, 939 (1992); J. L. Adams, W. W. Graessley, and R. A. Register, *ibid.* **27**, 6026 (1994); K. W. McKay, W. A. Gros, and C. F. Diehl, J. Appl. Polym. Sci. **56**, 947 (1995); B. L. Riise, G. H. Fredrickson, R. G. Larson, and D. S. Pearson, Macromolecules **28**, 7653 (1995).
[9] C. Y. Ryu, M. S. Lee, D. A. Hajduk, and T. P. Lodge, J. Polym. Sci., Part B: Polym. Phys. **35**, 2811 (1997).
[10] J. H. Laurer, D. A. Hajduk, J. C. Fung, J. W. Sedat, S. D. Smith, S. M. Gruner, D. A. Agard, and R. J. Spontak, Macromolecules **30**, 3938 (1997); A. Avgeropoulos, B. J. Dair, N. Hadjichristidis, and E. L. Thomas, *ibid.* **30**, 5634 (1997).
[11] Y. Matsushita, M. Nomura, J. Watanabe, Y. Mogi, I. Noda, and M. Imai, Macromolecules **28**, 6007 (1995).
[12] S.-M. Mai, W. Mingvanish, S. C. Turner, C. Chaibundit, J. P. A. Fairclough, A. J. Ryan, F. Heatley, and C. Booth (unpublished).
[13] A. M. Mayes and M. Olvera de la Cruz, J. Chem. Phys. **91**, 7228 (1989).
[14] A. M. Mayes and M. Olvera de la Cruz, J. Chem. Phys. **95**, 4670 (1991).
[15] M. W. Matsen and M. Schick, Macromolecules **27**, 187 (1994).
[16] H. Watanabe, Macromolecules **28**, 5006 (1995).
[17] E. Helfand, J. Chem. Phys. **62**, 999 (1975).
[18] M. W. Matsen and M. Schick, Phys. Rev. Lett. **72**, 2660 (1994).
[19] M. W. Matsen and F. S. Bates, Macromolecules **29**, 1091 (1996).
[20] F. Schmid, J. Phys.: Condens. Matter **10**, 8105 (1998).
[21] M. W. Matsen and F.S. Bates, J. Polym. Sci., Part B: Polym. Phys. **35**, 945 (1997).
[22] A. N. Semenov, Macromolecules **22**, 2849 (1989).
[23] S.H. Anastasiadis, H. Retsos, C. Toprakcioglu, A. Menelle, and G. Hadziioannou, Macromolecules **31**, 6600 (1998).
[24] K. R. Shull, A. M. Mayes, and T. P. Russell, Macromolecules **26**, 3929 (1993).
[25] A. N. Semenov, Macromolecules **26**, 6617 (1993).
[26] N. Koneripalli, R. Levicky, F. S. Bates, M. W. Matsen, S. K. Satija, J. Ankner, and H. Kaiser, Macromolecules **31**, 3498 (1998).
[27] T. Geisinger, M. Müller, and K. Binder, J. Chem. Phys. (in press).
[28] W. H. de Jeu, P. Lambooy, I. W. Hamley, D. Vaknin, J. S. Pedersen, K. Kjaer, R. Seyger, P. van Hutten, and G. Hadziioannou, J. Phys. II **3**, 139 (1993).
[29] B. Li and E. Ruckenstein, Macromol. Theory Simul. **7**, 333 (1998).
[30] A.-C. Shi, J. Noolandi, and R. C. Desai, Macromolecules **29**, 6487 (1996).
[31] M. Schwab and B. Stühn, Phys. Rev. Lett. **76**, 924 (1996); N. Sakamoto, T. Hashimoto, C. D. Han, D. Kim, and N. Y. Vaidya, Macromolecules **30**, 1621 (1997).
[32] L. Leibler, Macromolecules **13**, 1602 (1980).
[33] S. A. Brazovskii, Sov. Phys. JETP **41**, 85 (1975).
[34] G. H. Fredrickson and E. Helfand, J. Chem. Phys. **87**, 697 (1987).
[35] W. W. Maurer, F. S. Bates, T. P. Lodge, K. Almdal, K. Mortensen, and G. H. Fredrickson, J. Chem. Phys. **108**, 2989 (1998).
[36] S. Stepanow, Macromolecules **28**, 8233 (1995).
[37] D. C. Morse and G. H. Fredrickson, Phys. Rev. Lett. **73**, 3235 (1994); M. W. Matsen, J. Chem. Phys. **104**, 7758 (1996).
[38] R. R. Netz and M. Schick, Phys. Rev. Lett. **77**, 302 (1996).